International Journal of Heat and Mass Transfer 114 (2017) 225–237

Contents lists available at ScienceDirect

International Journal of Heat and Mass Transfer

journal homepage: www.elsevier.com/locate/ijhmt

Analysis of single phase, discrete and mixture models, in predicting nanofluid transport

Ahmed Albojamal, Kambiz Vafai *

Department of Mechanical Engineering, University of California, Riverside, Riverside, CA, United States

ARTICLE INFO

Article history:
Received 14 May 2017
Received in revised form 6 June 2017
Accepted 8 June 2017

Keywords:
Nanofluids
Forced convection
Discrete-phase model
Single-phase
Two-phase
Mixture model
Nanoparticles

ABSTRACT

A numerical investigation of developing forced convective heat transfer and pressure drop of nanofluid flow inside a tube subject to a constant wall heat flux boundary condition is presented. The single-phase homogenous and two different two-phase models: Lagrangian-Eulerian model or (discrete phase model) and mixture model are utilized with both constant and temperature dependent properties to further investigate and clarify the differences and evaluate the assumption of the single-phase model. The obtained results were subjected to an intensive comparison with the available experimental data and numerical works in the literature. The influence of some important parameters such as, source and sink terms, injected particle mass flow rate, slip velocity, particle forces, Reynolds number, constant or temperature dependent properties and particle concentration on the heat transfer and flow characteristics of nanofluids were determined and discussed in detail. It was observed that the two phase Lagrangian-Eulerian model (DPM) overestimated the heat transfer coefficient values and the results from the mixture model displayed an unrealistic increase in heat transfer particularly for high particle volume fraction. The proposed single phase approach revealed a very good agreement with the experimental data and the maximum difference in the average heat transfer coefficient between the single-phase and DPM was found to be 5.9% considering variable properties. The results also revealed that increasing the injected particle mass flow rate does not have a significant effect on the heat transfer coefficient values and that the particles move with the same velocity of the fluid. Furthermore, the heat transfer coefficient increases as the particle volume fraction and Reynolds number increases, but it is accompanied by a higher pressure drop and wall shear stress values. DPM model provides a reasonable prediction for the thermal behavior of the nanofluids transport, the single-phase approach with temperature dependent viscosity and thermal conductivity is an accurate way to analyze the transport of nanofluids while requiring less CPU usage and memory for predicting the enhancement in nanofluids convective heat transfer.

1. Introduction

Nanofluids have shown better heat transfer enhancement and energy saving over base fluids in thermal applications [1,2]. Typical nanofluids are mixture of conductive solid particles 1–100 nm in diameter suspended in a base fluid which can be used in several applications such as electronic cooling, heat exchangers, automotive and air conditioning. The thermal conductivity of the particle materials, such as Al_2O_3, CuO, Cu are typically several orders-of-magnitude higher than the base fluid. As such, even at low concentrations, they have shown significant increases in the heat transfer coefficient [2–6].

Numerical and experimental studies were carried out by many researchers to evaluate the effect of utilizing nanofluids as the working fluid to enhance the thermal performance. Some analytical and experimental results [4,7] show that using a nanofluid as the working fluid is an efficient method to reduce the thermal resistance and entropy generation in a heat pipe. Other experimental studies [8–11] have shown that nanofluids possess higher heat transfer characteristics than the base fluid particularly for small particle diameters. It has been observed [9] that the enhancement in the heat transfer coefficients in the developing region is higher than that in the developed region. However, classical correlations for pure fluids cannot properly estimate the enhancement in the forced convective heat transfer of nanofluids for both constant wall temperature and constant heat flux boundary conditions [12,13].

Numerical investigation of forced convective heat transfer for water-Al_2O_3 nanofluid inside a circular tube under constant wall

* Corresponding author.
E-mail address: Vafai@engr.ucr.edu (K. Vafai).

http://dx.doi.org/10.1016/j.ijheatmasstransfer.2017.06.030
0017-9310/

Nomenclature

$\vec{a}$	particle's acceleration
C_p	specific heat transfer, J/kg K
cst.	constant properties
D	tube diameter, m
d	nanoparticle diameter, m
F	body force, N
g	gravitational acceleration, m/s^2
Gz	Graetz number, $VD^2/\alpha L$
H	total enthalpy, kJ/kg
h	heat transfer coefficient, W/m^2 K
k	thermal conductivity, W/mK
L	tube length, m
m	mass, kg
Nu	Nusselt number, hD/k
P	pressure, Pa
Pr	Prandtl number, $C_p\mu/k$
q	wall heat flux, W/m^2
r	radial coordinate, m
r_0	tube radius, m
Re	Reynolds number, $\rho VD/\mu$
S_m, S_e	source and sink terms
T	fluid temperature, K
T^*	dimensionless temperature, $(T - T_w)/(T_b - T_w)$
t	time, s
V	velocity vector, m/s
V_{dr}	drift velocity, m/s
δV	cell volume, m^3
var.	variable properties
z	axial coordinate, m

Greek letters

α	thermal diffusivity, m^2/s
μ	dynamic viscosity, Pa s
ρ	density, kg/m^3
Φ	particle volume fraction
τ	wall shear stress, Pa
k_B	Boltzmann constant, 1.3807×10^{-23} J/K
υ	kinematic viscosity, m^2/s

Subscripts

av	average
b	bulk mean
bf	base fluid
i	inlet
m	mixture
n	total number of particles
nf	nanofluid
p	nanoparticle
w	wall
0	reference to inlet condition

heat flux were presented by several investigators [14–16]. A new concept of combined/hybrid nanofluids based on CNTs + Al_2O_3, was introduced by Nuim Labib et al. [17]. They used two-phase mixture model to study forced convective heat transfer under constant wall heat flux. Their results showed that the combined mixture tends to enhance the convective heat transfer significantly because CNTs shows higher shear thinning behavior which results in a thinner boundary layer. In addition, using Ethylene Glycol as a base fluid instead of water appears to be more efficient in enhancing the heat transfer. Moghadassi et al. [18] investigated Al_2O_3/water and hybrid nanofluids with 0.1% volume concentration flowing inside a horizontal tube for steady state laminar region (*Re* < 2300). Khanafer et al. [19] presented a critical investigation to study the effect of nanoparticle addition, temperature and nanoparticle size-dependence on the specific heat capacity of both conventional and molten salt-based nanofluids. A general correlation for Al_2O_3-water nanofluids that takes into account the effect of temperature, volume fraction and nanoparticle size was developed and verified. Buongiorno [20] theoretically studied the effect of nanoparticle thermal dispersion on the energy transfer of nanofluids by considering seven slip mechanisms that can produce a relative velocity between the nanoparticles and the base fluid.

In our study, we investigate forced convective flow of nanofluids inside a circular tube under constant wall heat flux boundary condition. Ansys Fluent software [21] is used to solve the governing equations by means of a finite volume method. Three models were carried out for the simulation: single-phase and two phase (which included both Eulerian-Lagrangian and mixture models) to evaluate the percentage difference in predicting the nanofluid heat transfer coefficient between the investigated models and the physical effects of some important parameters on the flow behavior for nanoparticles volume fraction from 1% to 4%, taking into account constant and temperature dependent thermophysical properties. The results were compared with the experimental data of Wen and Ding [9], Kim et al. [11] and the numerical work of Bianco et al. [14].

2. Thermophysical properties of the nanofluid for a single-phase model

Conventional heat transfer fluids such as water have inherently low thermophysical properties as compared to solids. Therefore, dispersing colloidal small conductive solid particles such as $AL_2O_3 \leq 100$ nm in diameter can enhance the thermophysical properties for the base fluid. The thermophysical properties for the base fluid and alumina particles are given in Table 1. Researchers have proposed several correlations that can allow calculating properties such as thermal conductivity, density, viscosity and heat capacity, but there are still issues [5] regarding the proper correlations for predicting thermal conductivity and viscosity within an acceptable range. Therefore, further studies need to be conducted in this field.

2.1. Nanofluid density and specific heat

Solid-liquid mixture equations for estimating the density and specific heat capacity of nanofluids were employed from the following equations [5,22–25]:

$$\rho_{nf} = (1-\phi)\rho_{bf} + \phi\rho_p \quad (1)$$

$$Cp_{nf} = (1-\phi)Cp_{bf} + \phi Cp_p \quad (2)$$

Table 1
Physical properties of the base fluid and nanoparticles at T_i = 293 K.

Properties	Water	Al_2O_3
C_p (J/kg K)	4182	733
k (W/m K)	0.6	36
ρ (kg/m^3)	998.2	3880
μ_{water} = 0.001003 kg/m s		

2.2. Nanofluid dynamic viscosity

2.2.1. Constant properties

For constant properties, the effective viscosity depends only on the volume fraction Φ. A least-square curve fitting, based on some experimental data available in the open literature was performed by Maïga et al. [26] leading to the following correlation:

$$\frac{\mu_{nf}}{\mu_{bf}} = 1 + 7.3\phi + 123\phi^2 \tag{3a}$$

2.2.2. Temperature dependent properties

The following correlations are used as given in [5]:

$$\begin{aligned} \mu_{nf} &= 2.9\cdot 10^{-7}T^2 - 2.0\cdot 10^{-4}T + 3.4\cdot 10^{-2} \quad \text{for } \Phi = 1\% \\ \mu_{nf} &= 3.4\cdot 10^{-7}T^2 - 2.3\cdot 10^{-4}T + 3.9\cdot 10^{-2} \quad \text{for } \Phi = 4\% \end{aligned} \tag{3b}$$

2.3. Nanofluid thermal conductivity

2.3.1. Constant properties

The same procedure used for the dynamic viscosity is employed. Therefore, for example for Al_2O_3 the following equation is considered [26]:

$$\frac{k_{nf}}{k_{bf}} = 1 + 2.72\phi + 4.97\phi^2 \tag{4a}$$

It should be noted that by constant properties we are referring to no variance with respect to temperature. The other aspects such as composition are taken into account.

2.3.2. Temperature dependent properties

The following equations are used as suggested by Bianco et al. [14] and Palm et al. [27]:

$$\begin{aligned} k_{nf} &= 0.003352\cdot T - 0.3708 \quad \text{for } \Phi = 1\% \\ k_{nf} &= 0.004961\cdot T - 0.8078 \quad \text{for } \Phi = 4\% \end{aligned} \tag{4b}$$

The physical properties of the base fluid as a function of temperature can be represented as given in Comsol Multiphysics software:

$$\mu_{bf} = 1.38 - 0.021224T + 1.36\cdot 10^{-4}T^2 - 4.6454\cdot 10^{-7}T^3 + 8.904\cdot 10^{-10}T^4 - 9.08\cdot 10^{-13}T^5 + 3.8457\cdot 10^{-16}T^6 \tag{5}$$

$$k_{bf} = -0.86908 + 0.0089488T - 1.5836\cdot 10^{-5}T^2 + 7.97543\cdot 10^{-9}T^3 \tag{6}$$

3. Boundary conditions, geometric configuration and grid independence study

A two dimensional (2D) axisymmetric geometry was considered with a very fine mesh near the tube wall to capture the near wall behavior of the nanofluid. A non-uniform quadratic mesh is used as shown in Fig. 1 with a relatively coarse mesh in the vicinity of the tube axis since the flow properties along the central portion is expected to change more gradually. The tube is chosen to be long enough to ensure a fully developed flow at the tube outlet section. The tube is subjected to a constant wall heat flux boundary condition with a uniform axial velocity and temperature profile for the inlet section. The nanofluid is composed of water and Al_2O_3 particles with an average size of 100 nm and different volume fractions. To perform a grid independence test, four grid densities 15 × 500, 25 × 1000, 50 × 1250 and 80 × 1400 were used as shown in Fig. 2. Graphs of local Nusselt number were observed for Re = 250 and q = 5000 W/m^2 as well as higher Reynolds numbers. There was less than 0.2% difference in the local Nusselt number between the largest grid (80 × 1400) and the second largest grid (50 × 1250). Therefore, the latter grid is selected for simulation.

4. Solution scheme

Two way coupling between the fluid and the solid phase is considered during the simulation. As such, the fluid can affect the particle motion by drag, and the particles can exchange momentum and energy with the continuous fluid. The code is based on finite volume method and the SIMPLE algorithm to couple pressure and the velocity fields. PRESTO scheme for pressure, QUICK for volume fraction and SECOND ORDER UPWIND for other parameters were considered to discretize the governing equations. Nanoparticles injected with two different mass flow rate values (1% and 4%) were considered. It was found that increasing the injected particle mass flow rate does not change the nanofluid heat transfer coefficient significantly.

For discrete phase model, the solver completes 220 flow iterations per DPM iteration for Φ = 1% and Φ = 4%. For each discrete-phase iteration, the particle trajectories were computed and the interphase exchange of the momentum, heat, and mass in each control volume were updated. These interphase exchange terms affect the continuous phase when the continuous phase iteration is performed. During the coupled calculation, ANSYS Fluent will perform the discrete phase iteration at specified intervals during the continuous-phase calculation. The coupled calculation continues until the continuous phase flow field no longer changes with further calculations. When convergence is reached, the discrete phase trajectories no longer change either, since changes in the discrete phase trajectories would result in changes in the continuous phase flow field [28].

5. Mathematical modeling

5.1. Homogenous single-phase approach

This approach assumes that the nanoparticles can be easily fluidized to reach the base fluid velocity, thus the nanofluid is taken as a homogenous fluid flow with enhanced thermophysical properties. Further, this model considers both liquid and particle phases are in thermal equilibrium and move with the same velocity [29]. The dimensional governing equations for steady state single-phase model are as follows [14,22,23,30]:

Continuity,

$$\nabla.(\rho_{nf}\vec{V}) = 0 \tag{7}$$

Momentum,

$$\nabla.(\rho_{nf}\vec{V}\,\vec{V}) = -\nabla P + \nabla.(\mu_{nf}\nabla\vec{V}) \tag{8}$$

and Energy,

$$\nabla.(\rho_{nf}\vec{V}\,CpT) = \nabla.(k_{nf}\nabla T) \tag{9}$$

5.2. Lagrangian-Eulerian approach (DPM)

In the Lagrangian-Eulerian model (or discrete-phase model) the continuous phase is treated as a continuum, while the dispersed phase is solved by tracking a large number of spherical particles. The dispersed phase can exchange momentum, mass and energy with the base fluid. A fundamental assumption made in this model is that the dispersed phase is sufficiently dilute such that particle-particle interaction is almost negligible. The fluid is considered to

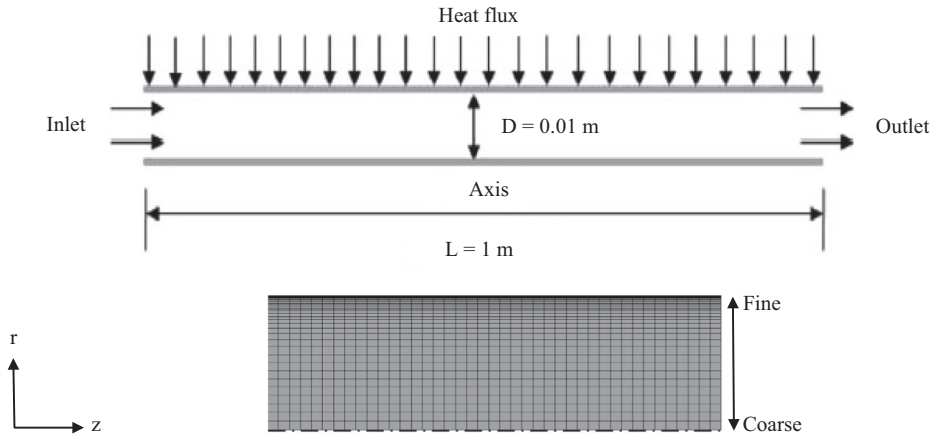

Fig. 1. Geometrical and mesh configurations for the current study.

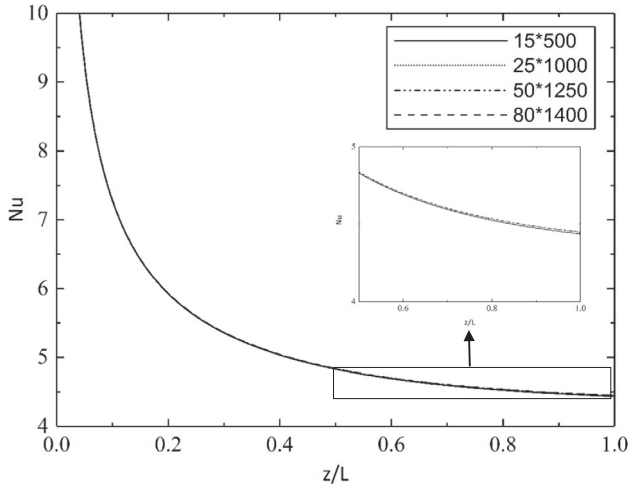

Fig. 2. Grid independence results.

be a single fluid with two phases, and the coupling between them is strong [28].

The following equations represent the mathematical formulation of Lagrangian-Eulerian two phase model [14,16,22]:

Continuity,

$$\nabla.(\rho_{nf}\vec{V}) = 0 \tag{10}$$

Momentum,

$$\nabla.(\rho_{nf}\vec{V}\vec{V}) = -\nabla P + \nabla.(\mu_{nf}\nabla\vec{V}) + S_m \tag{11}$$

and Energy,

$$\nabla.(\rho_{nf}\vec{V}CpT) = \nabla.(k_{nf}\nabla T) + S_e \tag{12}$$

In the DPM model, the solid phase (particles) and the fluid phase (base fluid) are simulated with a full two-phase method. The two sets of equations are linked by source/sink terms S_m and S_e which represent the integrated effects of the momentum and energy exchange with the base fluid as particles are moving through an element of Eulerian phase of the base fluid with volume of δV. The source and sink terms are updated after a certain number of base fluid iterations. These terms are identically equal to zero in the case of single-phase model.

The momentum exchange between the particles and the base fluid is calculated as [31]:

$$S_m = \frac{1}{\delta V}\sum_{p=1}^{n}\vec{F}_p \tag{13}$$

In the Lagrangian reference frame, the trajectories of particles are calculated by an integrating method and the force balance equates the particle inertia with the forces acting on the particle. The equation of motion of the particle is given by Eq. (14) as in Mirzaei et al. [31]:

$$m_p\frac{d\vec{V}_p}{dt} = F_D + F_g + F_L + F_{Br} + F_T + F_P + F_v \tag{14}$$

where $\vec{V}_p$ is the particle velocity, m_p is the particle mass and the right-hand side represents the forces acting on the particle which are resistance F_D, gravity F_g, Saffman's lift F_L, Brownian F_{Br}, Thermophoresis F_T, pressure gradient F_P and virtual mass forces F_v respectively. To solve Eq. (14), we have to specify the proper correlations for each force term as follows:

– Drag force F_D is determined by stokes' relationship for submicron particles which imposes a limitation for the model, because stokes relationship is valid for $Re_d \leq 0.1$, where Re_d is defined as [23]:

$$Re_d = \frac{\rho d_p|\vec{V}_p - \vec{V}_c|}{\mu} \tag{15}$$

and,

$$F_D = \frac{18\mu}{d_p^2\rho_p C_c}(\vec{V} - \vec{V}_p)m_p \tag{16}$$

where C_c is the Cunningham correction factor for the stokes' relationship [32]:

$$C_c = 1 + \frac{2\lambda}{d}(1.257 + 0.4e^{-(1.1d/2\lambda)}) \tag{17}$$

where $\lambda = 0.17$ nm is the mean free path for the base fluid and $\vec{V}_c$ is the continuous phase velocity.

– Gravity force F_g is defined as follows:

$$F_g = \frac{g(\rho_p - \rho)}{\rho} \tag{18}$$

– Saffman's lift force F_L is determined by [33]:

$$F_L = \frac{2Kv^{1/2}\rho d_{ij}}{\rho_p d_p(d_{lk}d_{lk})^{1/4}}(\vec{V} - \vec{V}_p) \tag{19}$$

where $K = 2.594$ is the constant coefficient of Saffman's lift force and d_{ij} is the rate deformation tensor defined as:

$$d_{ij} = \frac{1}{2}(u_{i,j} + u_{j,i}) \tag{20}$$

This form of the lift force is intended for small particle Reynolds numbers and is recommended only for sub-micron particles [21].

– Brownian force F_{Br} is calculated by [28]:

$$F_{Br} = \zeta_i \sqrt{\frac{\pi S_0}{\Delta t}} \tag{21}$$

where ζ_i are zero-mean, unit-variance-independent Gaussian random numbers and S_o is:

$$S_0 = \frac{216 \nu k_B T}{\pi^2 \rho d_p^5 \left(\frac{\rho_p}{\rho}\right) C_c} \tag{22}$$

where k_B is the Boltzmann constant.

– Thermophoresis force F_T is determined using the form suggested by Talbot et al. [34]:

$$F_T = \frac{6\pi d_p \mu^2 C_s \left(\frac{k}{k_p} + C_t K_n\right)}{\rho(1 + 3C_m K_n)\left(1 + 2\left(\frac{k}{k_p}\right) + 2C_t K_n\right)} \frac{1}{m_p T} \nabla T \tag{23}$$

where

K_n: Knudsen number = $2\lambda/d_p$

C_m: momentum exchange coefficient = 1.146

C_t: temperature jump coefficient = 2.18

C_s: thermal slip coefficient = 1.147

– Pressure gradient force F_p is given by:

$$F_p = \left(\frac{\rho}{\rho_p}\right) V_p . \nabla V \tag{24}$$

where V is the axial velocity.

Virtual mass force F_v, the force required to accelerate the fluid surrounding the particle is expressed as:

$$F_v = C_{vm} \frac{\rho}{\rho_p} \left(\vec{V}_p \nabla \vec{V} - \frac{d\vec{V}_p}{dt}\right) \tag{25}$$

where C_{vm} is the virtual mass factor with a default value of 0.5.

By solving Eq. (13), the momentum exchange S_m will be available through computing the change in the momentum of a particle as it passes through each control volume of the Eulerian base fluid. Because of the small scale and high thermal conductivity of nanoparticles, the particles can be considered as a lumped system. Therefore, the energy balance for a particle can be written as:

$$m_p Cp \frac{dT_p}{dt} = hA_p(T - T_p) \tag{26}$$

where, the heat transfer coefficient h is calculated from Ranz and Marshall's correlation [35]:

$$Nu = \frac{h \cdot d}{k} = 2 + 0.6 Re_d^{1/2} Pr^{1/3} \tag{27}$$

Once Eq. (26) is solved, it is possible to obtain the energy exchange following the same approach used for the momentum equation:

$$S_e = \frac{1}{\delta V} \sum_{p=1}^{n} m_p Cp \frac{dT_p}{dt} \tag{28}$$

The main assumption of the DPM approach is represented by the correlations used to evaluate the forces and heat transfer coefficient which were originally developed for the submicron particles.

5.3. Mixture model

This is a simplified multiphase model that uses a single fluid two-phase approach, by assuming the coupling between phases is strong, and a local equilibrium between the phases should be reached over a short spatial length scale. In this model, each phase has its own velocity vector field and within a given control volume there exists a certain fraction for each phase. In addition to continuity, momentum and energy equations, mixture model solves the volume fraction equation for the secondary phase. It then uses an algebraic expression to calculate the relative velocity between the phases.

The following dimensional equations represent the mathematical description of mixture model governing equations [15,17,33]:

Continuity,

$$\nabla . (\rho_m \vec{V}_m) = 0 \tag{29}$$

Momentum,

$$\nabla . (\rho_m \vec{V}_m \vec{V}_m) = -\nabla P + \nabla . (\mu_m \nabla \vec{V}_m) + \nabla . \left(\sum_{k=1}^{n} \phi_k \rho_k \vec{V}_{dr,k} \vec{V}_{dr,k}\right) \tag{30}$$

Energy,

$$\nabla . \sum_{k=1}^{n} (\phi_k \vec{V}_k (\rho_k H_k + P)) = \nabla . (k \nabla T) \tag{31}$$

and Volume fraction equation,

$$\nabla . (\phi_p \rho_p \vec{V}_m) = -\nabla . (\phi_p \rho_p \vec{V}_{dr,p}) \tag{32}$$

where $\vec{V}_m$, ρ_m, μ_m and H_k are expressed as:

$$\vec{V}_m = \frac{\sum_{k=1}^{n} \phi_k \rho_k \vec{V}_k}{\rho_m} \tag{33}$$

$$\rho_m = \sum_{k=1}^{n} \phi_k \rho_k \tag{34}$$

$$\mu_m = \sum_{k=1}^{n} \phi_k \mu_k \tag{35}$$

$$H_k = h_k - \frac{P}{\rho_k} + \frac{v_k^2}{2} \tag{36}$$

In the momentum equation (30) $\vec{V}_{dr,k}$ is the drift velocity for the secondary phase k (i.e., nanoparticles) which is defined as:

$$\vec{V}_{dr,k} = \vec{V}_k - \vec{V}_m \tag{37}$$

The relative velocity (slip velocity) is defined as the velocity of the secondary phase (p) relative to the velocity of the primary phase (base fluid):

$$\vec{V}_{pf} = \vec{V}_p - \vec{V}_f \tag{38}$$

The drift velocity is related to the relative velocity as follows:

$$\vec{V}_{dr,p} = \vec{V}_{pf} - \sum_{k=1}^{n} \frac{\phi_k \rho_k}{\rho_m} \vec{V}_{fk} \tag{39}$$

The relative velocity $\vec{V}_{pf}$ in the above equation is calculated from Eq. (40) proposed by Manninen et al. [36]:

$$\vec{V}_{pf} = \frac{\rho_p d_p^2}{18 \mu_m f_{drag}} \frac{(\rho_p - \rho_m)}{\rho_p} \vec{a} \tag{40}$$

where the drag function, f_{drag}, is determined by Schiller and Naumann's correlation [37]:

$$f_{drag} = \begin{cases} 1 + 0.15Re_p^{0.687} & Re_p \leqslant 1000 \\ 0.0183Re_p & Re_p \geqslant 1000 \end{cases} \quad (41)$$

The acceleration in Eq. (40) can be expressed as:

$$\vec{a} = \vec{g} - (\vec{V}_m \cdot \nabla)\vec{V}_m$$

In this model, only one set of velocity components is solved from the differential equations for the mixture momentum, while the velocity of the dispersed phase is obtained from the algebraic balance equations. Also, it is important to note that the primary phase impresses the secondary phase via drag, while the secondary phase in turn influences the primary phase via reduction in the mean momentum. In addition, the continuity, momentum and energy equations are solved for the whole mixture rather than utilizing the governing equations for each phase independently.

6. Results and discussion

Results were first obtained for pure water flow inside a circular tube to evaluate the accuracy and reliability of the grid distribution and the model. The obtained local Nusselt number was validated with a correlation presented by Churchill and Ozoe [38] with an average deviation of under 2% as shown in Fig. 3 for thermally and hydraulically developing flow with a uniform heat flux of 5000 W/m^2. The Churchill and Ozoe [38] correlation is as follows:

$$\frac{Nu_D}{4.364\left[1+\left(\frac{Gz}{29.6}\right)^2\right]^{\frac{1}{6}}} = \left[1+\left(\frac{\frac{Gz}{19.04}}{\left[1+\left(\frac{Pr}{0.0207}\right)^{2/3}\right]^{\frac{1}{2}}\left[1+\left(\frac{Gz}{29.6}\right)^2\right]^{\frac{1}{3}}}\right)^{3/2}\right]^{\frac{1}{3}} \quad (42)$$

Eq. (42) agrees within 5% with other investigators numerical data for $Pr = 0.7$ and $Pr = 10$ [39].

Next, laminar flow of Al_2O_3/water nanofluid is considered with particle diameter $d_p = 100$ nm. Three different models were used in the numerical simulation: single-phase homogenous and two phase (Lagrangian-Eulerian and mixture) models for three different particle loadings ($\Phi = 1\%$, $\Phi = 3\%$ and $\Phi = 4\%$ by volume) and $Re = 250$, 500, 750, 1050 and 1460 with three different constant wall heat flux boundary conditions, q = 5000, 7500 and 10,000 W/m^2 considering both constant and temperature dependent properties. The results were compared with experimental and numerical data available in the open literature.

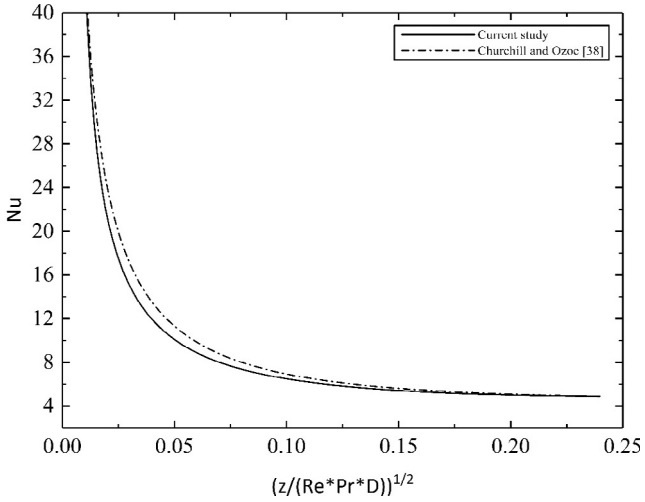

Fig. 3. Model validation with Churchill and Ozoe's correlation [38].

Fig. 4(a) and (b) shows the comparison of the wall and bulk fluid temperature profiles along the tube axis with Bianco et al.'s [14] numerical results for q = 5000 W/m^2 and R = 250 for constant and temperature dependent properties. The average differences in the wall temperature between single-phase model and DPM for $\Phi = 1\%$ and $\Phi = 4\%$ and variable properties were 0.15% and 0.001% respectively, while the maximum discrepancy between the present study and Bianco et al. [14] was found to be 4.3% at tube exit for the discrete phase model for $\Phi = 1\%$. However, the converged solution was kept at the very low relative tolerance of 10^{-6} for all of the equations. If the tolerance was increased to around 10^{-3} for the continuity equation, the wall temperature profiles for all the models would coincide with Bianco et al. [14] results. The fluid bulk temperature decreases appreciably with the augmentation of the particle volume fraction since the nanoparticles have a beneficial effect on the thermal properties of the resulting mixture. For example, the product ρC_p increases as much as 7.8% for $\Phi = 4\%$ with respect to the base fluid at $\Phi = 0\%$. Therefore, introducing the nanofluid decreases the wall and bulk temperatures over the base fluid as shown in Fig. 4(a).

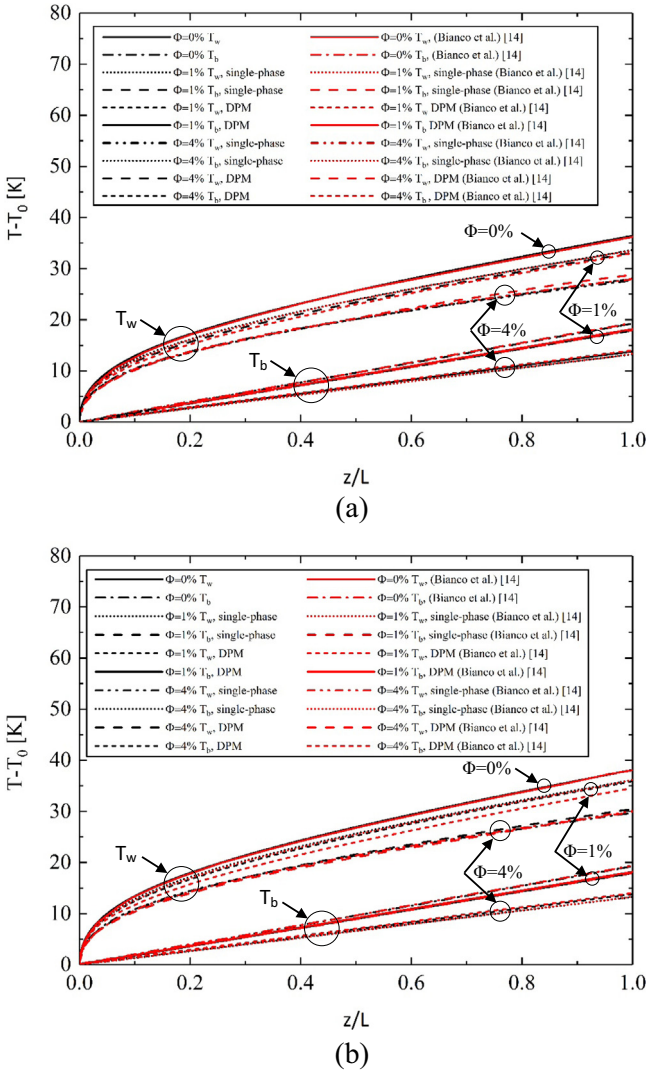

Fig. 4. Comparison of the wall and bulk temperature profiles along the tube axis with Bianco et al. [14] for different volume fractions: (a) Temperature dependent properties and (b) constant properties.

There is a significant difference between the constant and variable properties results in Bianco et al. [14] study, as also reported in Özerinç et al. [12]. Fig. 5(a) and (b) shows the temperature profiles across the tube cross section at z/L = 0.99 m for Φ = 1% and Φ = 4% and the investigated models for the two cases. It can be noticed that the difference between the base fluid and nanofluid temperature dramatically increases as the tube radius and volume fraction increases, indicating that higher heat transfer rates with nanoparticles is achieved. In the vicinity of the tube wall, it is important to consider a very fine mesh to predict the change in the wall temperature accurately. Adding nanoparticles to the base fluid can change the radial temperature profile, but it is clear from the figure that the single phase model can predict the temperature distribution very well in comparison with the two-phase model for constant and temperature dependent properties where the average deviation between the investigated models for temperature dependent properties for Φ = 1% and Φ = 4% are 1.3% and 1.8% respectively. However, in Fig. 5 the maximum discrepancy between the current study and Bianco et al. [14] occurs at Φ = 1% for constant properties mostly because we used relatively finer mesh in the area around the center line and the tube wall. Our results show that the nanoparticles have a tendency to migrate toward the tube centerline for developing region, while in fully developed region nanoparticles follow the streamlines and remain parallel as shown in Fig. 6(a). It is clearly observed that the velocity profile and hydrodynamic entrance length are independent of the concentration values and that the nanoparticles move with the fluid velocity.

Fig. 6(b) shows a comparison of the dimensionless radial velocity profiles for the current work with those of Bianco et al. [14] for a volume fraction of Φ = 4% along the tube radius at different axial locations for *Re* = 250 and q = 5000 W/m^2. The hydrodynamic entry length is given by $L_{h,laminar} = 0.06\ Re_D\ D$ which is equivalent to z = 0.15 m from the inlet section. It can be observed that the nanofluid flow is fully developed at z = 0.16 m. It should be noted that the dimensional axial velocity profile for the nanofluid increases with an increase in the volume fraction for the same Reynolds number because the density and viscosity of the nanofluid are the two properties which are directly proportional to the nanoparticle volume fraction. Therefore, different nanoparticle volume fractions have different mean velocities to enable the Reynolds number to remain constant. It should be noted that the nanofluid viscosity increases at a substantially faster rate with an increase in nanoparticle concentration as compared to the density. The results are in good agreement with Bianco et al. [14].

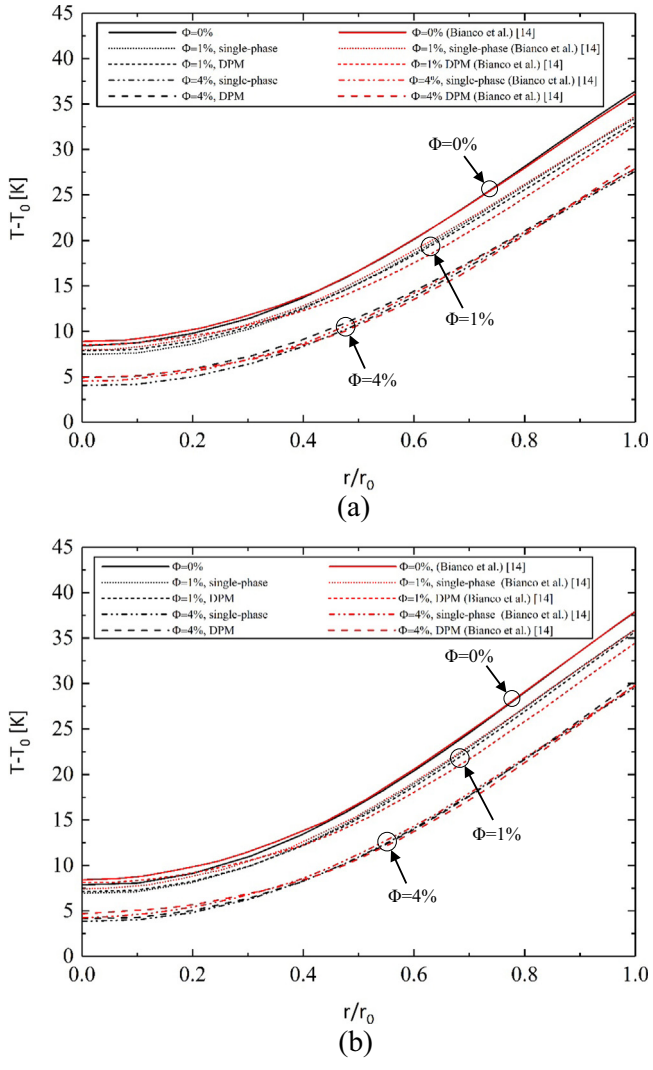

Fig. 5. Comparison of the temperature profile along the tube radius at z/L = 0.99 m for different volume fractions for q = 5000 W/m^2 and *Re* = 250 with Bianco et al. [14]: (a) Temperature dependent properties and, (b) constant properties.

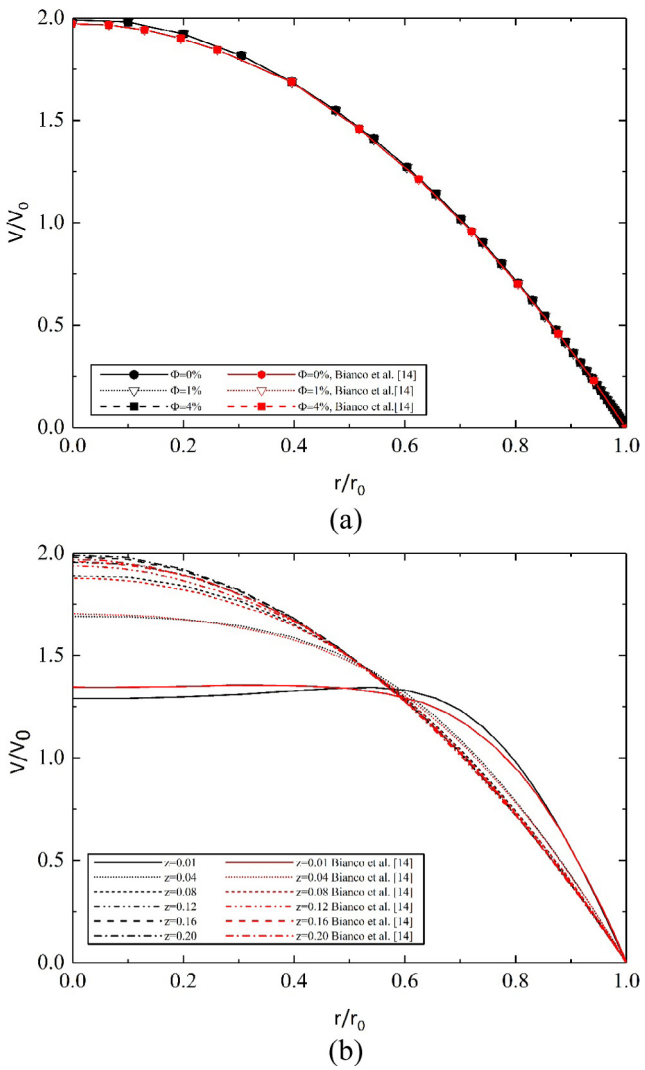

Fig. 6. Comparison of the radial velocity profiles for the current work with those of Bianco et al. [14] for q = 5000 W/m^2, *Re* = 250 and: (a) z = 0.2 m, (b) Φ = 4%.

Fig. 7(a) and (b) shows the comparison of the dimensionless temperature profiles for Φ = 0% and Φ = 4% at several tube locations respectively. A reduction of 2.5% in the dimensionless temperature profile at z = 0.9 m over the base fluid Φ = 0% can be seen, indicating a better heat transfer rate between the wall and the fluid. Also, it can be observed that when the particle volume fraction increases the Prandtl number increases resulting in a longer thermal entrance length. The results are in excellent agreement with Bianco et al. [14].

As mentioned earlier, particle volume fraction influences the physical properties and increases the mixture thermal conductivity. As such, the wall to fluid convective heat transfer would be consequently more important, as it is clearly shown in Fig. 8(a) where there is a higher increase in the average heat transfer coefficient. Particularly when Φ = 4% and *Re* = 1050 an enhancement of 25.97% in h_{av} with respect to the base fluid Φ = 0% can be seen. The difference between the single phase and two phase models are higher in the case of temperature dependent properties as shown in Fig. 8(b). The maximum discrepancies between the single-phase and discrete phase models for Φ = 1% and Φ = 4% considering variable properties are 5.9% and 3.2% respectively, while 5.5% and 4.6% respectively for constant properties. However, two-phase mixture model shows an unrealistic increase in the average heat transfer for small changes of the particle volume fraction because its thermal predictions are quite different from the other models as shown in Fig. 9. The total enthalpy in Eq. (31) for the mixture model increases significantly compared to others resulting in high heat transfer values. However, in case of Bianco et al.'s [14] study, 12.3% differences are detected between the single phase and discrete phase model for Φ = 1% and constant properties. Particularly, the two-phase model leads to overestimated values. Considering variable properties, the nanofluid simulation can give more accurate results specifically for high volume fraction Φ > 1%, since it will incorporate the changes in the thermal conductivity of the nanofluid with temperature. Our results were found to be in good agreement with the numerical work of Bianco et al. [14].

The effect of increasing injected particle mass flow rate from 1% to 4% of the fluid as a function of Reynolds number are shown in Fig. 10. It is clearly observed that increasing particle mass flow rate would not change the average heat transfer coefficient for the nanofluid significantly.

In the single phase model the effect of gravity, drag on particles and additional forces are omitted. However, these forces are present for the case of two phase model [6] as source and sink terms

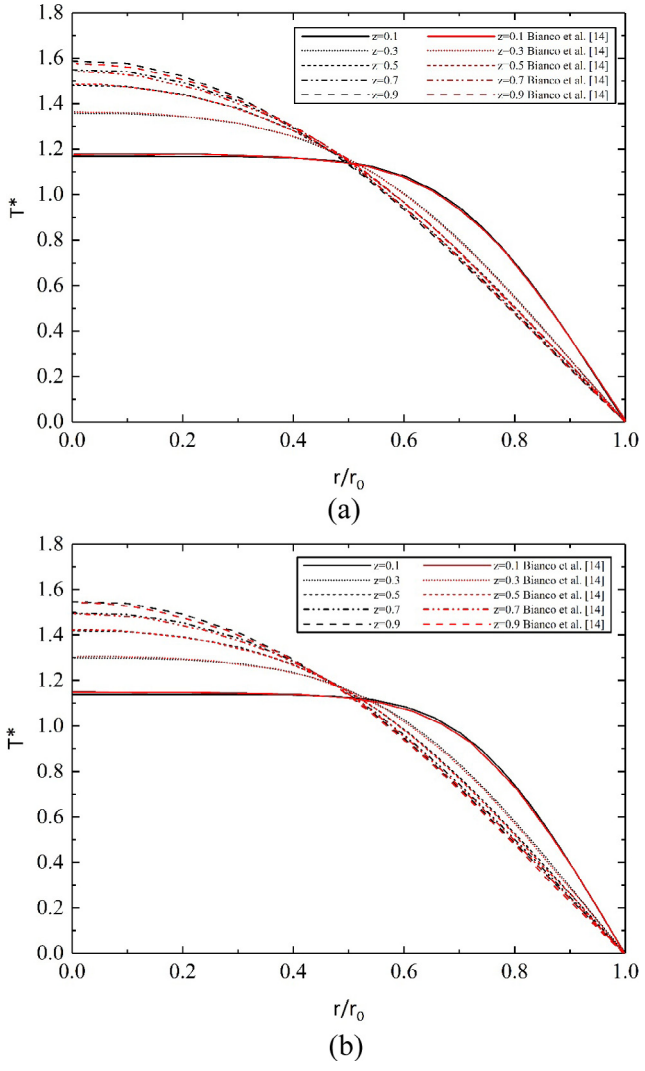

Fig. 7. Comparison of the dimensionless temperature for the current work with those of Bianco et al. [14] for q = 5000 W/m^2 and *Re* = 250 at different axial locations for: (a) Φ = 0%, (b) Φ = 4%.

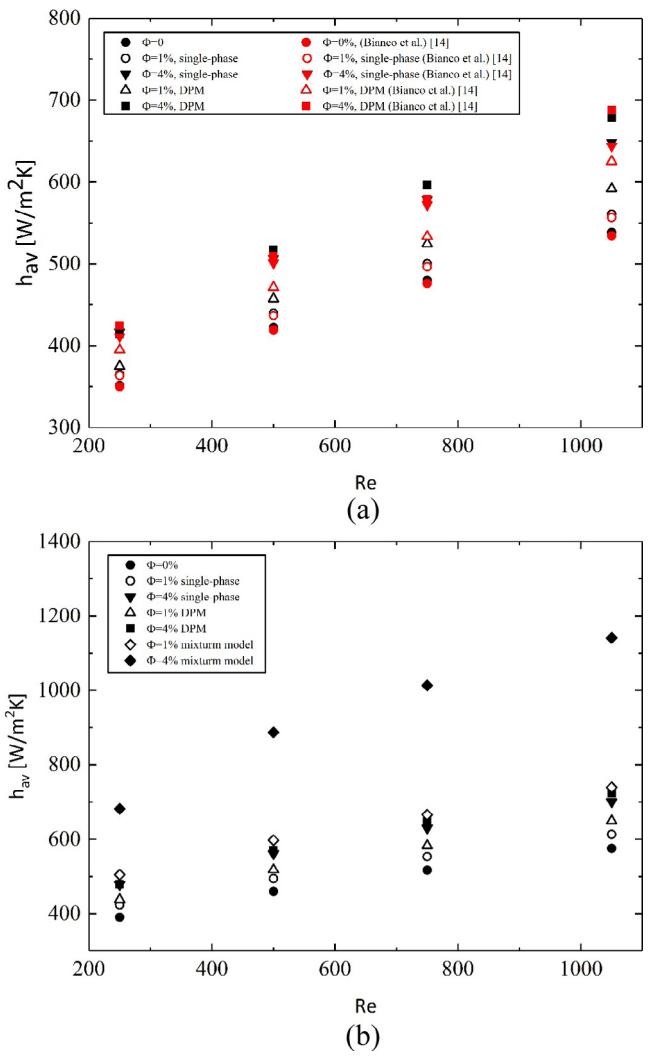

Fig. 8. Average heat transfer coefficient as a function of Reynolds number for q = 1000 W/m^2 and *Re* = 250: (a) constant properties and comparison of current results with those of Bianco et al. [14], (b) variable properties.

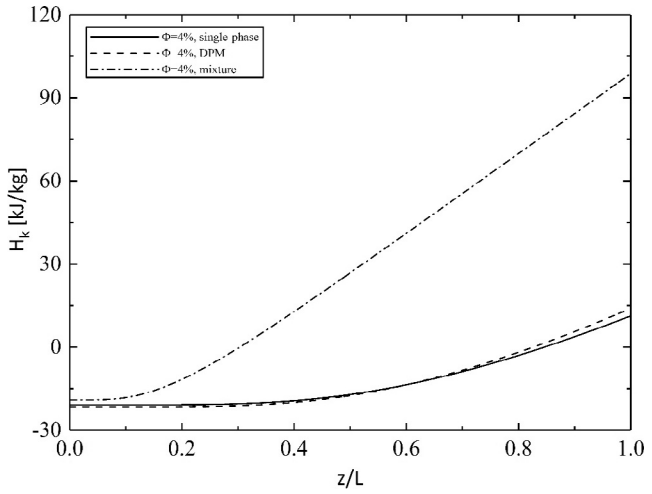

Fig. 9. Total enthalpy along the axial direction for $Re = 250$, q = 10,000 W/m^2 for different models.

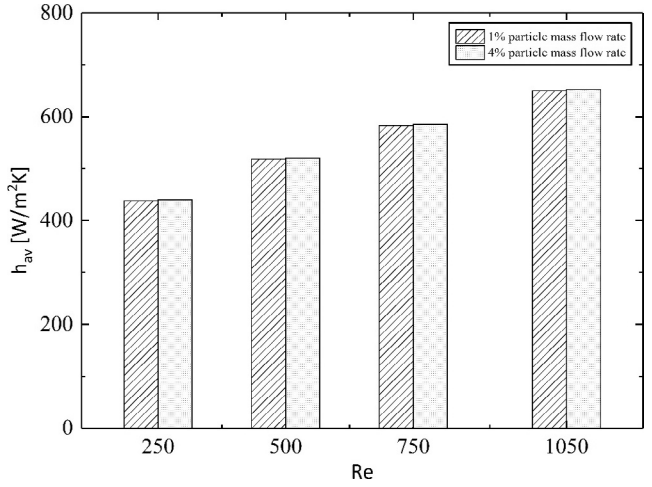

Fig. 10. Effect of the injected particle mass flow rate on the nanofluid average heat transfer coefficient as a function of Reynolds number for q = 10,000 W/m^2, Φ = 1% and DPM.

in the momentum and energy equations. As such, they may affect the wall temperature and ultimately the heat transfer coefficient. As such, the physical effects of the additional forces on the average heat transfer coefficient were considered in this study and reported in Table 2. It is clearly seen that the additional force terms do not play a significant role in the results regardless of the imposed heat flux. Therefore, they can be ignored when nanoparticles are considered.

As was shown earlier, the average heat transfer coefficient for the single-phase model is quite similar to that of the discrete phase model as shown in Fig. 8(b). The percentage difference in the average relative heat transfer coefficient between the investigated models is shown in Table 3 for Φ = 1% and Φ = 4% respectively. A maximum discrepancy of 5.9% was found between the single-phase model and DPM. When variable properties are taken into account the percentage difference decreases appreciably when particle volume fraction becomes 4%. However, the two-phase mixture model shows higher enhancement in nanofluids heat transfer particularly, for high particle volume fraction which makes it unreliable in predicting the values within an acceptable range. The single phase homogenous model shows a good agreement in modeling heat transfer in nanofluids. We had established that the effect of both source and additional force terms can be ignored.

To show the reliability of the single-phase model assumption, two comparisons with the experimental data of Wen and Ding [9] for local heat transfer coefficient for $Re = 1050$ and Φ = 1% and Kim et al. [11] for $Re = 1460$ and Φ = 3% for Al_2O_3/water nanofluid flow inside a circular tube subject to a constant wall heat flux were carried out as shown in Fig. 11(a) and (b) respectively. It can be observed from Fig. 11(a) that the mixture model can only predict heat transfer values for low particle volume fractions $\Phi \leq 1\%$ and for the developing region, while the numerical results from the single-phase model are in a good agreement with the measured data for the fully developed region z/D > 66. The maximum discrepancy with the experimental data is 5% at z/D = 116 for the single-phase model, whereas, the average difference between the single-phase and the two-phase (DPM) models is less than 7%.

Comparison with the recent experimental work of Kim et al. [11] shows that the numerical results from the single-phase model provide an excellent prediction for the nanofluid local heat transfer coefficient with an average error of 1.1% while mixture model failed in estimating the heat transfer values. It is important to note that the difference between the single-phase and DPM is relatively negligible as the volume fraction increases as shown in Fig. 11(b) and Table 3(b). In Fig. 12(a) comparison is carried out for the average Nusselt number for Φ = 1% and different Reynolds numbers for constant and temperature dependent properties. The results from the single-phase model for constant and variable properties show a good agreement with Bianco et al. [14] and the correlation provided by Maïga et al. [26] with a maximum deviation for $Re = 250$.

For the case of $Re = 250$ the maximum discrepancies between the single-phase constant properties and single-phase variable properties is 4.4%. This difference decreases as the volume fraction increases to Φ = 4%. Fig. 12(b) shows that, the results from the single-phase variable properties are in excellent agreement with DPM with a maximum deviation of 3.2% for the case of $Re = 1050$ while the mixture model deviates much more over the whole range of Reynolds numbers.

The temperature gradient can result in a significant decrease in the viscosity within the boundary layer leading to the heat transfer enhancement [19] as can be seen in Fig. 13(a) and (b). The substantial increase in heat transfer coefficient at the entry region and the enhancement strongly depends on the particle volume fraction. An average enhancement of 19.6% and 6.8% in heat transfer coefficient for Φ = 4% and Φ = 1% respectively over the base fluid can be seen in Fig. 13(c) for variable properties and 3.8% and 18.6% for constant properties. The results are in good agreement with Bianco et al. [14] and the maximum discrepancy of 2% in heat transfer coeffi-

Table 2
Effect of additional forces on the average heat transfer coefficients for a particle concentration of Φ = 1%.

q (W/m^2)	*Re*	Percentage increase h_{nf} [$F_{specific}$]/h_{nf}					
	Physical effect	Lift	Brownian	Thermophoretic	Pressure	Virtual	All
5000	250	1.56735E−05	0.002769446	2.97536E−05	0.00000	0.00000	0.002022
	750	7.95093E−05	0.001694321	4.12632E−05	1.27901E−06	6.83377E−05	0.002344
	1050	2.54463E−05	0.000816116	8.22296E−05	2.26011E−05	2.30535E−05	0.00218

Table 3
Average values of h_{nf}/h_{bf} for *Re* = 250 and different heat fluxes for (a) Φ = 1%, (b) Φ = 4%.

q (W/m^2)	Single-phase model (SPM)		DPM		Mixture model		DPM perc. difference % compared to SPM		Mixture model perc. difference% compared to SPM	
	Cst.	Var.	Cst.	Var.	Cst.	Var.	Cst.	Var.	Cst.	Var.
(a) Φ = 1%										
5000	1.038	1.068	1.063	1.106	1.358	1.357	2.394	3.580	30.841	27.093
7500	1.038	1.079	1.063	1.122	1.347	1.333	2.404	3.926	29.782	23.489
10,000	1.038	1.084	1.067	1.122	1.347	1.351	2.783	3.476	29.776	24.583
(b) Φ = 4%										
5000	1.186	1.196	1.190	1.218	1.898	1.805	0.388	1.843	60.077	50.960
7500	1.185	1.213	1.190	1.211	1.898	1.815	0.392	0.099	60.097	49.702
10,000	1.186	1.226	1.190	1.228	1.898	1.824	0.395	0.183	60.090	48.792

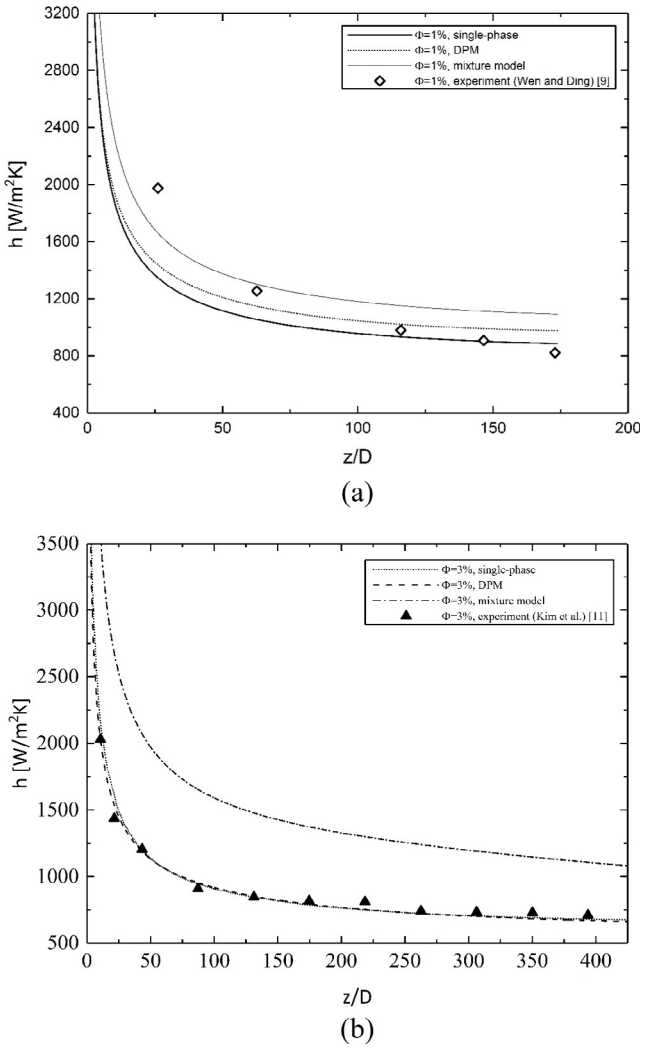

Fig. 11. Comparison of the present results with the experimental data of: (a) Wen and Ding [9], (b) Kim et al. [11].

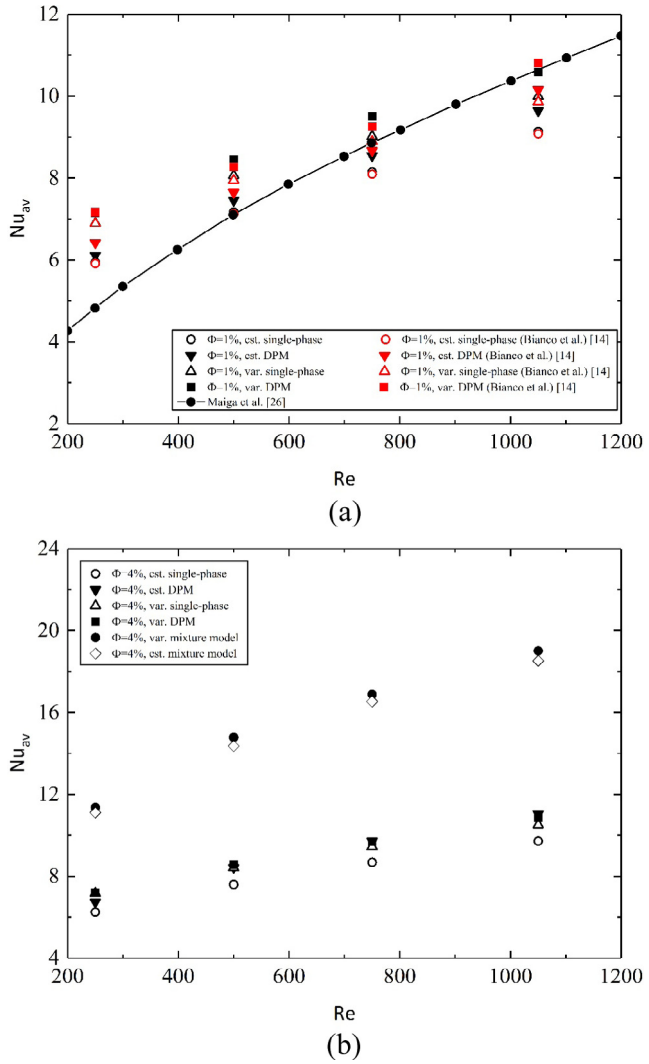

Fig. 12. Average Nusselt number as a function of Reynolds for: (a) Φ = 1%, (b) Φ = 4%.

cient for a volume fraction of Φ = 1% for the constant property case. The two-phase (DPM) model slightly overestimates the heat transfer coefficient specifically for low volume fractions as shown in Fig. 13(d) and reported in Table 4, while two-phase mixture model provides an unrealistic value. Also, it can be clearly observed from Fig. 13(c) that the difference between the constant and variable properties increases along the tube axis for all values of the volume fractions, which means that the constant property assumption could give an erroneous result particularly for low volume fractions i.e., Φ < 1%.

However, as the temperature increases the viscosity near the wall decreases due to the higher temperature gradient leading to lower wall shear stresses for variable property assumption as

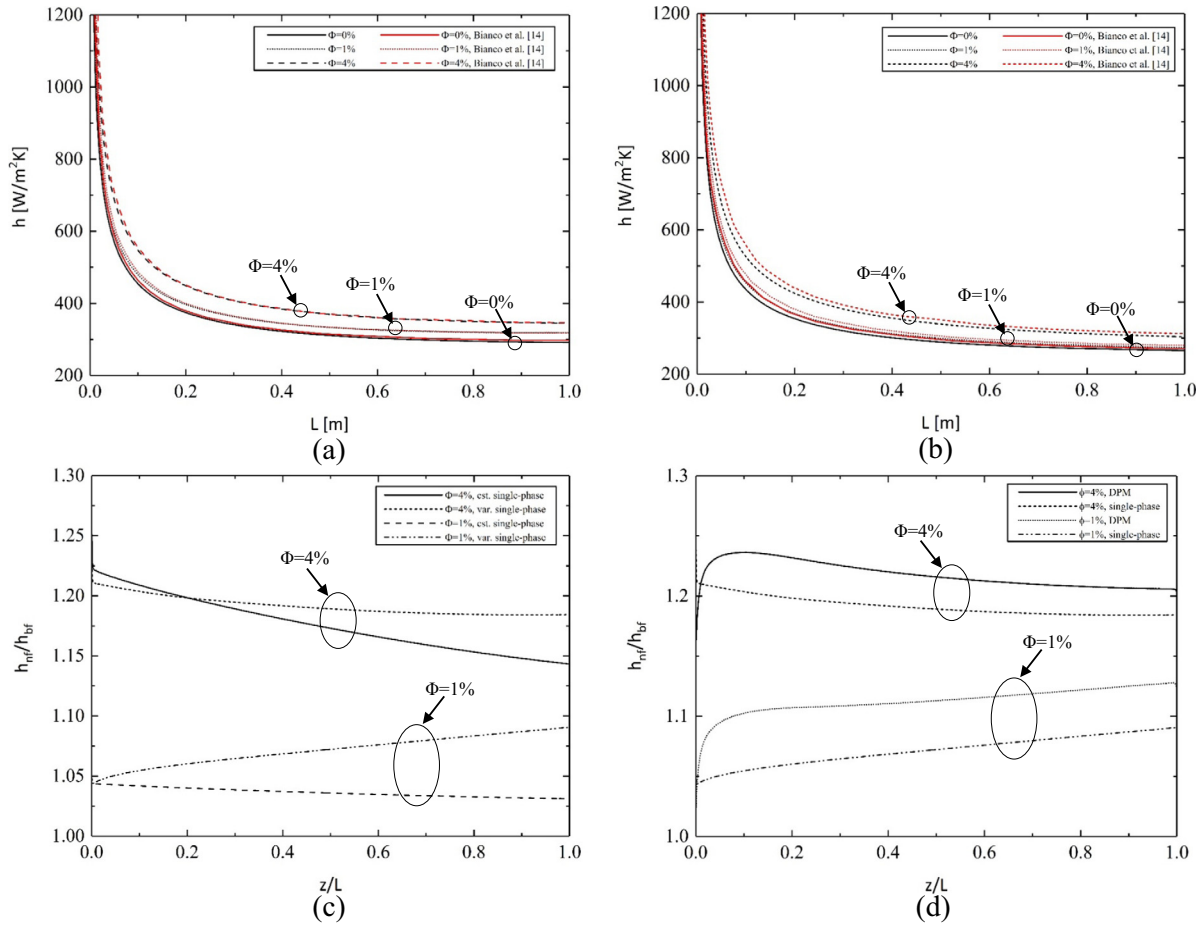

Fig. 13. Heat transfer enhancement along the axial direction for $Re = 250$ and $q = 5000\ W/m^2$: (a) variable properties, (b) constant properties, (c) single phase model, (d) difference between single phase and two phase models for variable properties.

Table 4
Average and relative heat transfer coefficients for $Re = 250$ and $q = 5000\ W/m^2$ for different models.

Model		Φ(%)	h_{av} [W/m²K]	h_{nf}/h_{bf}	Nu_{av}	Nu_{nf}/Nu_{bf}
H_2O	Cst.	0	351.420	1	5.886	1
	Var.		373.734	1	6.260	1
Single-phase	Cst.	1	364.771	1.038	6.110	1.038
	Var.		399.024	1.068	6.684	1.068
DPM	Cst.	1	373.505	1.063	6.256	1.063
	Var.		413.310	1.106	6.923	1.106
Mixture model	Cst.	1	477.275	1.358	7.995	1.358
	Var.		507.131	1.357	8.495	1.357
Single-phase	Cst.	4	416.650	1.186	6.979	1.186
	Var.		446.967	1.196	7.487	1.196
DPM	Cst.	4	418.269	1.190	7.006	1.190
	Var.		455.206	1.218	7.625	1.218
Mixture model	Cst.	4	666.966	1.898	11.172	1.898
	Var.		674.744	1.805	11.302	1.805

shown in Table 5 where an average wall shear stress for different particle concentrations for $Re = 250$ and $q = 5000\ W/m^2$ is reported. When the particle concentration increases the average shear stress also increases. For all of the cases studied here, the values from constant properties are higher than those from variable properties and values from the two phase DPM model are higher than those for the single-phase model.

An average increment of 16.9% and 120% in pressure drop for the volume fractions of $\Phi = 1\%$ and $\Phi = 4\%$ respectively over the base fluid $\Phi = 0\%$ was observed in Fig. 14. Addition of nanoparticles increases the density and viscosity of the nanofluid and consequently results in a pressure drop penalty. Thus, larger values of particle volume fraction can influence the pressure drop remarkably and restricts their applications for the thermal systems work-

Table 5
Average wall shear stress for Re = 250 and q = 5000 W/m^2 for different models.

Model		Φ (%)	τ_{av} (Pa)	τ_{nf}/τ_{bf}
H_2O	Cst.	0	0.020	1
	Var.		0.015	1
Single-phase	Cst.	1	0.023	1.145
	Var.		0.017	1.185
DPM	Cst.	1	0.032	1.571
	Var.		0.024	1.630
Mixture model	Cst.	1	0.031	1.533
	Var.		0.026	1.795
Single-phase	Cst.	4	0.041	2.008
	Var.		0.030	2.032
DPM	Cst.	4	0.050	2.476
	Var.		0.041	2.836
Mixture model	Cst.	4	0.030	1.489
	Var.		0.026	1.795

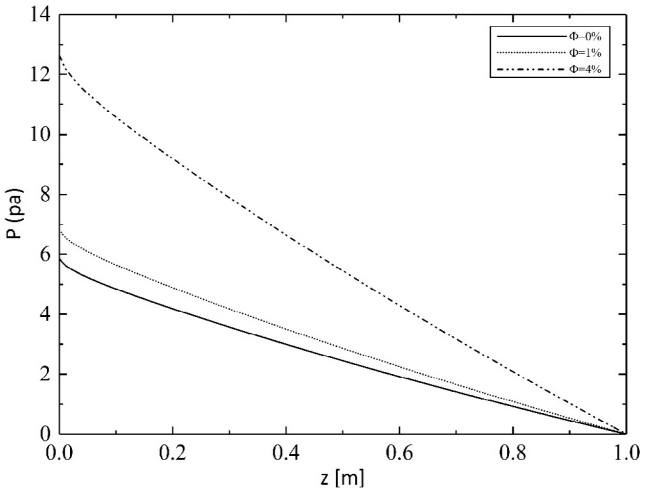

Fig. 14. Pressure drop along the axial direction for different volume fractions.

ing under limited pumping power condition [29], such as the case for electronic cooling.

7. Conclusions

Three different models were analyzed in the current study: single-phase, mixture and discrete phase models considering both constant and temperature dependent properties to investigate differences in hydrodynamic and thermal characteristics between the cited models for nanofluids transport. Results when variable properties were taken into account displayed higher heat transfer enhancements and Nusselt numbers for nanofluids. The maximum deviation between single-phase and DPM was found to be 5.9%. Results also displayed that the two-phase mixture model did not properly predict the heat transfer results when variable properties were taken into account. It was found that, particles follow the fluid streamlines and the effect of additional forces on particles can be ignored, particularly for $1\% < \Phi \leq 4\%$. In terms of the computational time and CPU usage, due to poor convergence criteria for DPM since the entire residual jumps up at each update of source terms in momentum and energy equations to obtain a converged solution, it took a far longer time for the continuity equation to reach the convergence limit with thousands of iterations, while the single-phase model could provide the results within few minutes. The results for the heat transfer coefficient showed that inclusion of nanoparticles provided considerable enhancement over the base fluid. However, nanofluids introduced a pressure drop penalty and increased the wall shear stress. The results clearly established that the single-phase model could provide a fast and low cost method for analyzing nanofluids, since it only requires information about the mixture thermophysical properties without reference to the particles and the base fluid separately. A comprehensive comparison was done with the experimental and numerical works and it was found that the single-phase model is in a good agreement with the experimental data from Kim et al. [11] and Wen and Ding [9] and Maïga et al.'s [26] correlation and numerical study of Bianco et al. [14]. The number of source term updates in DPM simulations had a significant impact in increasing the required CPU time. It was established that the single-phase model can predict nanofluids transport attributes within an acceptable range without the need for using the two-phase models.

Conflict of interest

There is no conflict of interest. This manuscript has not been submitted to anywhere else.

References

[1] S.U.S. Choi, J.A. Eastman, Enhancing thermal conductivity of fluids with nanoparticles, in: D.A. Singer, H.P. Wang (Eds.), Developments and Applications of Non-Newtonian Flows, vol. 231, ASME, New York, 1995, pp. 99–105.
[2] S. Kakaç, A. Pramuanjaroenkij, Review of convective heat transfer enhancement with nanofluids, Int. J. Heat Mass Transfer 52 (13–14) (2009) 3187–3196.
[3] K. Khanafer, K. Vafai, M. Lightstone, Buoyancy-driven heat transfer enhancement in a two-dimensional enclosure utilizing nanofluids, Int. J. Heat Mass Transfer 46 (19) (2003) 3639–3653.
[4] M. Ghanbarpour, R. Khodabandeh, K. Vafai, An investigation of thermal performance improvement of a cylindrical heat pipe using Al_2O_3 nanofluid, Heat Mass Transfer (2016).
[5] K. Khanafer, K. Vafai, A critical synthesis of thermophysical characteristics of nanofluids, Int. J. Heat Mass Transfer 54 (19–20) (2011) 4410–4428.
[6] M. Shafahi, V. Bianco, K. Vafai, O. Manca, Thermal performance of flat-shaped heat pipes using nanofluids, Int. J. Heat Mass Transfer 53 (7–8) (2010) 1438–1445.
[7] K. Alizad, K. Vafai, M. Shafahi, Thermal performance and operational attributes of the startup characteristics of flat-shaped heat pipes using nanofluids, Int. J. Heat Mass Transfer 55 (1–3) (2012) 140–155.
[8] K.B. Anoop, T. Sundararajan, S.K. Das, Effect of particle size on the convective heat transfer in nanofluid in the developing region, Int. J. Heat Mass Transfer 52 (9–10) (2009) 2189–2195.
[9] D. Wen, Y. Ding, Experimental investigation into convective heat transfer of nanofluids at the entrance region under laminar flow conditions, Int. J. Heat Mass Transfer 47 (24) (2004) 5181–5188.
[10] S. Suresh, K.P. Venkitaraj, P. Selvakumar, M. Chandrasekar, Effect of Al_2O_3–Cu/water hybrid nanofluid in heat transfer, Exp. Therm. Fluid Sci. 38 (2012) 54–60.
[11] D. Kim, Y. Kwon, Y. Cho, C. Li, S. Cheong, Y. Hwang, S. Ellipsis Moon, Convective heat transfer characteristics of nanofluids under laminar and turbulent flow conditions, Curr. Appl. Phys. 9 (2) (2009) e119–e123.
[12] S. Özerinç, A.G. Yazıcıoğlu, S. Kakaç, Numerical analysis of laminar forced convection with temperature-dependent thermal conductivity of nanofluids and thermal dispersion, Int. J. Therm. Sci. 62 (2012) 138–148.
[13] K.S. Hwang, S.P. Jang, S.U.S. Choi, Flow and convective heat transfer characteristics of water-based Al_2O_3 nanofluids in fully developed laminar flow regime, Int. J. Heat Mass Transfer 52 (1–2) (2009) 193–199.
[14] V. Bianco, F. Chiacchio, O. Manca, S. Nardini, Numerical investigation of nanofluids forced convection in circular tubes, Appl. Therm. Eng. 29 (17–18) (2009) 3632–3642.
[15] R. Lotfi, Y. Saboohi, A.M. Rashidi, Numerical study of forced convective heat transfer of nanofluids: comparison of different approaches, Int. Commun. Heat Mass Transfer 37 (1) (2010) 74–78.
[16] M. Keshavarz Moraveji, E. Esmaeili, Comparison between single-phase and two-phases CFD modeling of laminar forced convection flow of nanofluids in a circular tube under constant heat flux, Int. Commun. Heat Mass Transfer 39 (8) (2012) 1297–1302.
[17] M. Nuim Labib, M.J. Nine, H. Afrianto, H. Chung, H. Jeong, Numerical investigation on effect of base fluids and hybrid nanofluid in forced convective heat transfer, Int. J. Therm. Sci. 71 (2013) 163–171.

[18] A. Moghadassi, E. Ghomi, F. Parvizian, A numerical study of water based Al_2O_3 and Al_2O_3–Cu hybrid nanofluid effect on forced convective heat transfer, Int. J. Therm. Sci. 92 (2015) 50–57.
[19] K. Khanafer, F. Tavakkoli, K. Vafai, A. AlAmiri, A critical investigation of the anomalous behavior of molten salt-based nanofluids, Int. Commun. Heat Mass Transfer 69 (2015) 51–58.
[20] J. Buongiorno, Convective transport in nanofluids, J. Heat Transfer 128 (3) (2006) 240–250.
[21] ANSYS® Academic Research, Release 18.0, 2016.
[22] S.M. Vanaki, P. Ganesan, H.A. Mohammed, Numerical study of convective heat transfer of nanofluids: a review, Renew. Sustain. Energy Rev. 54 (2016) 1212–1239.
[23] C. Press, Heat Transfer Enhancement with Nanofluids, Edited by Vincenzo Bianco, Oronzio Manca, Sergio Nardini, and Kambiz Vafai, 2015.
[24] S.M.S. Murshed, K.C. Leong, C. Yang, Enhanced thermal conductivity of TiO_2—water based nanofluids, Int. J. Therm. Sci. 44 (4) (2005) 367–373.
[25] Bock Choon Pak, Young I. Cho, Hydrodynamic and heat transfer study of dispersed fluids with submicron metallic oxide particles, Exp. Heat Transfer 11 (2) (1998) 151–170.
[26] S.E.B. Maïga, S.J. Palm, C.T. Nguyen, G. Roy, N. Galanis, Heat transfer enhancement by using nanofluids in forced convection flows, Int. J. Heat Fluid Flow 26 (4) (2005) 530–546.
[27] S.J. Palm, G. Roy, C.T. Nguyen, Heat transfer enhancement with the use of nanofluids in radial flow cooling systems considering temperature-dependent properties, Appl. Therm. Eng. 26 (17–18) (2006) 2209–2218.
[28] ANSYS® Academic Research, release 18.0, Help System, 24.6.1.2 Coupled Calculations, ANSYS, Inc., 2016.
[29] L. Godson, B. Raja, D. Mohan Lal, S. Wongwises, Enhancement of heat transfer using nanofluids—an overview, Renew. Sustain. Energy Rev. 14 (2) (2010) 629–641.
[30] M.K. Moraveji, R.M. Ardehali, CFD modeling (comparing single and two-phase approaches) on thermal performance of Al_2O_3/water nanofluid in mini-channel heat sink, Int. Commun. Heat Mass Transfer 44 (2013) 157–164.
[31] M. Mirzaei, M. Saffar-Avval, H. Naderan, Heat transfer investigation of laminar developing flow of nanofluids in a microchannel based on Eulerian-Lagrangian approach, Can. J. Chem. Eng. 92 (6) (2014) 1139–1149.
[32] A. Li, G. Ahmadi, Dispersion and deposition of spherical particles from point sources in a turbulent channel flow, Aerosol Sci. Technol. 16 (4) (1992) 209–226.
[33] M.S. Mojarrad, A. Keshavarz, A. Shokouhi, Nanofluids thermal behavior analysis using a new dispersion model along with single-phase, Heat Mass Transfer 49 (9) (2013) 1333–1343.
[34] L. Talbot, R.K. Cheng, R.W. Schefer, D.R. Willis, Thermophoresis of particles in a heated boundary layer, J. Fluid Mech. 101 (04) (1980) 737.
[35] W.J. Minkowycz, E.M. Sparrow, J.Y. Murthy, Handbook of Numerical Heat Transfer, second ed., April 2006.
[36] M. Manninen, V. Taivassalo, S. Kallio, On the Mixture Model for Multiphase Flow, vol. 288, VTT Publications, 1996, pp. 3–67.
[37] L. Schiller, A. Naumann, A drag coefficient correlation, Z. Ver. Deutsch. Ing. 77 (1935) 318–320.
[38] S.W. Churchill, H. Ozoe, Correlations for laminar forced convection with uniform heating in flow over a plate and in developing and fully developed flow in a tube, J. Heat Transfer 95 (1) (1973) 78.
[39] A. Bejan, Convection Heat Transfer, fourth ed., Wiley, Hoboken, NJ, 2013.